Applied Surface Science 626 (2023) 157281

Contents lists available at ScienceDirect

Applied Surface Science

journal homepage: www.elsevier.com/locate/apsusc

Full Length Article

SERS substrates based on rose petal replicas for the oxidative stress detection

M. Barshutina [a,*], N. Doroshina [a], A. Baizhumanov [b], E. Nikelshparg [b], A. Fedotova [b,c], A. Popov [d,c], A. Semyanov [c,d], D. Yakubovsky [a], G. Tselikov [a], O. Luneva [b], I. Kirilyuk [e], G. Maksimov [b], V. Volkov [a], A. Arsenin [a], N. Brazhe [b,*], S. Novikov [a,*]

[a] Center for Photonics and 2D Materials, Moscow Institute of Physics and Technology, Dolgoprudny, Russia
[b] Faculty of Biology, Moscow State University, Leninskie Gory, Moscow, Russia
[c] Shemyakin-Ovchinnikov Institute of Bioorganic Chemistry, Russian Academy of Sciences, Moscow, Russia
[d] Department of Physiology, Jiaxing University College of Medicine, Jiaxing, China
[e] Vorozhtsov Novosibirsk Institute of Organic Chemistry SB RAS, Novosibirsk, Russia

ARTICLE INFO

Keywords:
Biosensors
Nano- and micropatterned surfaces
SERS substrate
Plasmonic nanostructures
Erythrocytes
Blood diagnostics

ABSTRACT

Oxidative stress leads to multiple changes in properties of cells and of biological liquids that can cause various pathologies including cardiovascular and metabolic diseases. Modern test systems make it possible to assess the concentration of oxidized molecules in the blood plasma, but do not provide direct information about oxidation of cell membranes. In this work, we presented an effective, scalable, and inexpensive technique for manufacturing biomimetic SERS sensors for the detection of biomembrane oxidation. The main feature of this technique is the use of rose petals as templates for scalable manufacturing of SERS substrates with a cavity structure that promotes the capture and immobilization of blood cells on the grooved inner surfaces of microcavities. To obtain the SERS effect in these microcavities, the silicone replicas of rose petals were covered with an Au thin film (100 nm) and spherical Au nanoparticles by the sequential deposition and annealing processes. The application of SERS substrates with a cavity structure enables to perform studies on individual erythrocytes and detect first signs of their membrane oxidation, which can be used for early diagnostics of various blood and metabolic diseases.

1. Introduction

The development of personalized medicine and early-stage diagnostics requires new highly sensitive and selective techniques based on the use of new materials and methodological approaches. One of such approaches is based on monitoring the development of oxidative stress in the blood cells.

Oxidative stress develops due to the high amount of reactive oxygen species (ROS) that are excessively generated inside cells and/or cannot be detoxified by the defense antioxidant systems. Due to their high reactivity, ROS interact with lipids, proteins, DNA, and RNA, causing various damages that compromise cell health and contribute to disease development, including cancer, vascular, and metabolic disorders. Modern diagnostic testing systems can be used to assess the level of some ROS and products of ROS interaction with cell molecules in biological liquids, but they cannot provide information about the oxidative stress-related damage of cell membranes and can be misleading in the result interpretation [1–3]. To monitor the oxidative stress development and to detect the cell damage as a marker of oxidative stress, we propose a new highly sensitive technique based on the use of surface-enhanced Raman spectroscopy (SERS) and a biomimetic approach.

SERS is a powerful and versatile tool in chemical and biochemical diagnostics [4–6]. This technique exploits the effect of surface plasmon resonance and unique molecular vibrational modes to identify the structure of analytes down to the single-molecule level. In the last decade, it has been demonstrated that SERS can also be used to perform

Abbreviations: ROS, reactive oxygen species; SERS, surface-enhanced Raman spectroscopy; AuNPs, gold nanoparticles; HFD, high-fat diet; EPR, electron paramagnetic resonance; TMT-H, 1-Hydroxy-4-isobutyramido-2,2,6,6-tetramethylpiperidinium chloride; Hb, hemoglobin; RSD, relative standard deviation; SEM, scanning electron microscopy; PDMS, polydimethylsiloxane; Hb_{mb}, membrane-bound hemoglobin.

* Corresponding authors.
E-mail addresses: barshutina.mn@mipt.ru (M. Barshutina), nadezda.brazhe@biophys.msu.ru (N. Brazhe), novikov.s@mipt.ru (S. Novikov).

https://doi.org/10.1016/j.apsusc.2023.157281
Received 15 December 2022; Received in revised form 5 April 2023; Accepted 13 April 2023
Available online 17 April 2023
0169-4332/

studies on individual cells, bacteria, and viruses in their natural environments [7–9]. Generally, a colloidal-based SERS approach is preferred for studies of such microscale objects due to a Raman signal of higher intensity compared to flat SERS substrates [10,11]. Previously, the colloidal-based approach has even been used for SERS studies of erythrocyte membranes [12]. However, its widespread use is highly limited due to a hypoosmolar effect of a colloidal solution on cells and to a low reproducibility of the obtained signal. Various factors, such as surface chemistry, charge, adsorbed molecules, external environment, and dynamic interaction between target and colloidal nanoparticles, can compromise the stability of SERS colloids, resulting in constant fluctuations of a detected SERS signal [13].

To improve reliability of a SERS signal at a single-cell level while maintaining its high intensity, several research groups proposed to use solid SERS substrates covered with microcavity structures [14–16]. Such microcavities promote the immobilization of cells on their inner surfaces and provide a significant enhancement of SERS signal intensity due to the increase in the effective contact area of a cell membrane with plasmonic nanoparticles located on the inner surface of microcavities [14].

So far, several highly technological techniques have been applied to produce SERS surfaces with microcavity structures, including X-ray/UV lithography, etching, electroplating, molding, etc. [17–19]. However, these methods commonly require complex and costly fabrication processes with highly sophisticated templates, which is crucial for their transfer from laboratory prototyping to mass production. To address these issues, a number of research teams proposed to use biological surfaces patterned with complex hierarchical microstructures as templates for cheap and scalable SERS substrate manufacturing.

For instance, two research groups fabricated SERS sensors based on lotus and rose petals covered with silver nanoparticles [20,21]. Other groups used silicone replicas of rose, taro, gladiolus, and banana leaves or petals to produce microstructured SERS substrates for the detection of low molecular weight compounds such as Rhodamine 6G, malachite green, and herbicide detection [22–24]. However, the applicability of such biomimetic substrates to the analysis of high molecular weight compounds and large biological objects such as cells has not been studied yet.

In this work, we demonstrated that a similar biomimetic approach can be used to obtain SERS sensors for living cell analysis, which is highly promising for various biological and medical applications. One of the main challenges in the implementation of this strategy was choosing a biological surface with a microcavity structure that promotes the capture and immobilization of studied cells. Upon a thorough study of various biological surfaces (plant leaves, flower petals, insect wings, etc.), we revealed that negative replicas of rose petals are most effective for the capture and immobilization of blood cells, which have been the subject of our research for many years. In our previous work [25–27], we demonstrated that SERS of red blood cells is a useful tool for detecting even early signs of such metabolic diseases as diabetes, hypertension, obesity, etc. So, the development of an effective and inexpensive technology for mass production of SERS sensors capable of even single erythrocyte analysis is of great practical importance for medicine and biology. To achieve this goal, we proposed a biomimetic technique inspired by a microstructure of rose petals. The detailed description of this technique and experimental proof of its effectiveness for manufacturing of highly sensitive single-cell SERS sensors are given below.

2. Materials and methods

2.1. Manufacturing the silicone substrates with a cavity structure

The fabrication of biomimetic silicone substrates was performed by a soft lithography technique. A silicone elastomer for the rose petal replication was prepared using commercially available Sylgard-184 (Dow Corning, Midland, MI, USA) with a base/curing agent mixing ratio of 10:1. Fresh roses (*Rose Hybrid Tea*) of four different colors (white, pink, yellow, and red) were purchased from the local market. Several pieces (~2 cm^2) of each rose were fixed in a petri dish and poured with liquid silicone that was allowed to cure for 2 days at 20 °C. Then silicone replicas were peeled off using tweezers and washed with distilled water.

2.2. Fabrication of plasmonic nanostructures on silicone replicas of rose petals

The layered structure of Au/SiO_2/Au (with respective thickness of 100 nm/5 nm/ 6.5 nm) was deposited on silicone replicas of rose petals by a Nano Master NEE-4000 electron beam evaporation system (Nano-Master, Austin, TX, USA) at a high vacuum (~10^{-6} Torr) and room temperature (23 °C) with a deposition rate of 0.5–1 A/s. The nominal thickness of deposited Au and SiO_2 films was controlled by a built-in quartz oscillator sensor. Then, silicone substrates with a deposited Au/SiO_2/Au films were annealed in a CVD Oxford PlasmaLab 100 chamber (Oxford Instruments, Abingdon, UK) at 550 °C and high-vacuum (~10^{-6} Torr) for 15 min to obtain isolated spherical Au nanoparticles (AuNPs) uniformly distributed on a SiO_2 surface. The size of obtained particles is variated from diameter of 30–60 nm.

2.3. Preparation of erythrocytes

All procedures were performed in accordance with the European Communities Council Directive (2010/63/EU) and approved by the Institute of Bioorganic Chemistry ethical committee. Animals were kept under standard housing conditions with a reversed 12-h light/dark cycle with free access to water and food. The 2- to 3-month-old C57BL/6 mice were divided into control and high-fat diet (HFD) groups. The HFD group received the fat-enriched chow (Sniff Diets, Soest, Germany) and the control animals had the standard chow for 2 months prior to the blood sampling. Each group consisted of 5 animals. 50 μl of blood was taken from the tail vein of control mice and mice on HFD and was fully saturated with oxygen before experiments. Blood was 2.000 times diluted with the physiological saline for erythrocytes (saline composition in mM: 145 NaCl, 5 KCl, 4 Na_2HPO_4, 1 NaH_2PO_4, 1 $MgSO_4$, 1 $CaCl_2$, pH 7.4). The obtained diluted blood was immediately placed on SERS substrates, and experiments were run in 1–2 min to ensure erythrocytes attachment to the surface of SERS structures.

2.4. Preparation of liposomes

Liposomes were prepared from fresh raw egg yolk using the method from [28] with minor modifications. Oxidative stress in liposomes was induced by means of the Fenton reaction according to the protocol described in [29]. The estimation of ROS amount in the control liposome samples and the samples after the Fenton reaction was performed by electron paramagnetic resonance (EPR) spectroscopy with a ROS-sensitive spin probe 1-Hydroxy-4-isobutyramido- 2,2,6,6-tetramethylpiperidinium chloride (TMT-H) [30]. EPR spectra were recorded at 25°C with a RE-1307 EPR spectrometer (Analitpribor, Smolensk, Russia) at the microwave power and time constant of 22 mW and 0.1 s, respectively. The concentration of TMT-H in liposome samples was 0,1 MM, and incubation time before measurements was 15 min. For each sample, 10 EPR spectra were recorded. The qualitative estimation of ROS amount was done by the intensity of the central line in TMT-H EPR spectra (I_0). To perform SERS measurements on control and oxidized liposomes, we used two-times diluted (with the phosphate buffer solution) liposome suspensions prepared from the initial liposome sample and from the liposomes incubated with H_2O_2 and $FeSO_4$ for 30 min.

2.5. SERS measurements

SERS experiments were performed using a confocal scanning Raman

microscope Horiba LabRAM HR Evolution (Horiba, Kyoto, Japan) equipped with a linearly polarized laser 532 nm, spot size of ~0.43 μm, and 600 lines/mm diffraction grating. The laser wavelength was chosen at 532 nm due to the resonance absorbance of hemoglobin (Hb) at this wavelength, so the influence of scattering from transmembrane proteins or cytoskeleton on the measuring signal can be neglected. All the spectra were collected using the ×50 objective (NA = 0.75) and 10 s of integration time. Laser power on a sample was 3.5 mW. The mean values of SERS spectra and their relative standard deviations (RSD) were calculated from 6 independent measurements in each case.

2.6. Reflectivity measurements

The reflection spectra of the fabricated substrates were recorded by a Biolam M-1 microscope (LOMO, St. Petersburg, Russia) in a backscattering configuration, equipped with a halogen light source, polarizers, and a fiber-coupled grating spectrometer QE65000 (Ocean Optics, Orlando, FL, USA) with a wavelength resolution of 1.6 nm and an objective magnification of 100x (NA = 0.8). The microscope images (1600 × 1200 pixels) were captured with an optical microscope (Nikon LV150L, Tokyo, Japan) equipped with a color digital camera DS-Fi3.

2.7. SEM measurements

The scanning electron microscopy (SEM) (JSM-7001F, JEOL, Tokyo, Japan) was used for the visualization of micro- and nanostructures on substrate surfaces.

3. Results and discussions

3.1. Fabrication and SEM analysis of biomimetic SERS substrates

The entire fabrication process of biomimetic SERS substrates is demonstrated in Fig. 1.

Rose petals of four different colors (white, pink, yellow, and red) were used as master molds to produce silicone substrates patterned with microcavity structures (Fig. S1 and S2). Here, silicone rubber or polydimethylsiloxane (PDMS) was chosen for the replication due to its high-level flexibility, extensibility, and outstanding biological properties. The use of PDMS enabled us to obtain high resolution replicas of rose petals that can be easily peeled off without any apparent damage. The SEM studies of rose petal surfaces and their silicone replicas confirmed the accuracy of replication.

According to SEM images of rose petals (Fig. 2a,b), their surface is covered with periodic convex structures (20–30 μm in diameter) separated by a web of trenches (~2 μm in width). At the top of these convex structures, there are submicron cuticular foldings (0.8–1.0 μm in width) that spread from the center to the edge. On the other hand, the inverted silicone replicas of rose petals (Fig. 2c-d). demonstrated that their surface is covered with honeycomb-like cavities of corresponding sizes with submicron foldings at their walls and bottom. Furthermore, PDMS replicas of red, yellow, pink, and white rose petals exhibited similar cavity structure, but different cavity depths (Fig. S3). To ensure that roses of the same color have the same microstructure of their petal surfaces, rose petals taken from a dozen roses of each color were examined.

The deposition of Au/SiO_2/Au layers on the obtained silicone replicas with a subsequent annealing of the upper gold layer resulted in the formation of the complex hierarchical structure (Fig. 2e,f). Notably, the coating of silicone replicas with Au and SiO_2 thin films does not significantly affect replica micromorphology since the resulting thickness of coating layers is only about 100 nm (Fig. 2e). However, the highly magnified SEM images of the coated silicone replicas (Fig. 2f) demonstrated that golden nanoparticles of predominantly round shape and various sizes (from 10 to 60 nm) have formed on the walls and bottom of honeycomb-like cavities as a result of the upper gold layer annealing (Fig. S4). Thus, the obtained SERS substrates exhibit the hierarchical structure consisting of microcavities, submicron foldings, and gold nanostructures of ranging sizes which is highly promising for a SERS analysis of living cells due to the favorable conditions for multiple reflection and scattering of electromagnetic waves.

3.2. Reflectivity properties of biomimetic SERS substrates

The optical properties of biomimetic SERS substrates were characterized by reflection spectroscopy before and after the annealing process (Fig. S5). According to the obtained results (Fig. S5a), the reflectance

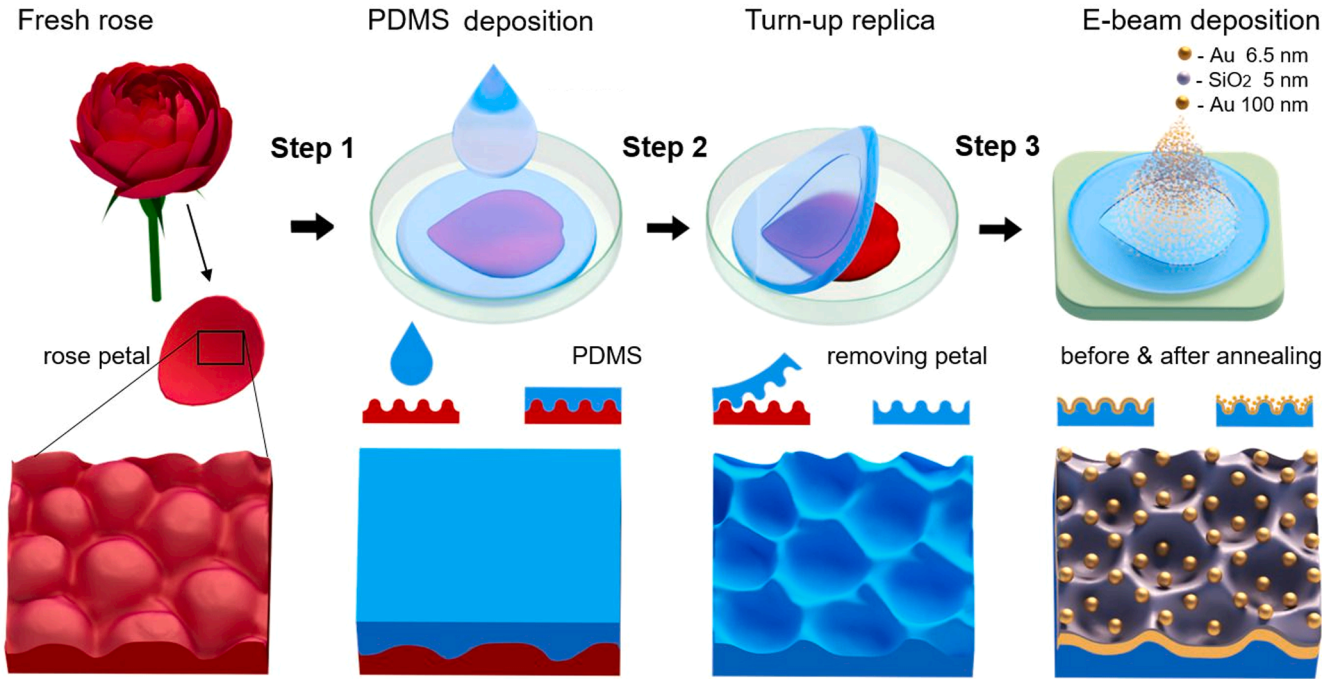

Fig. 1. The schematic illustration of manufacturing the biomimetic SERS substrates.

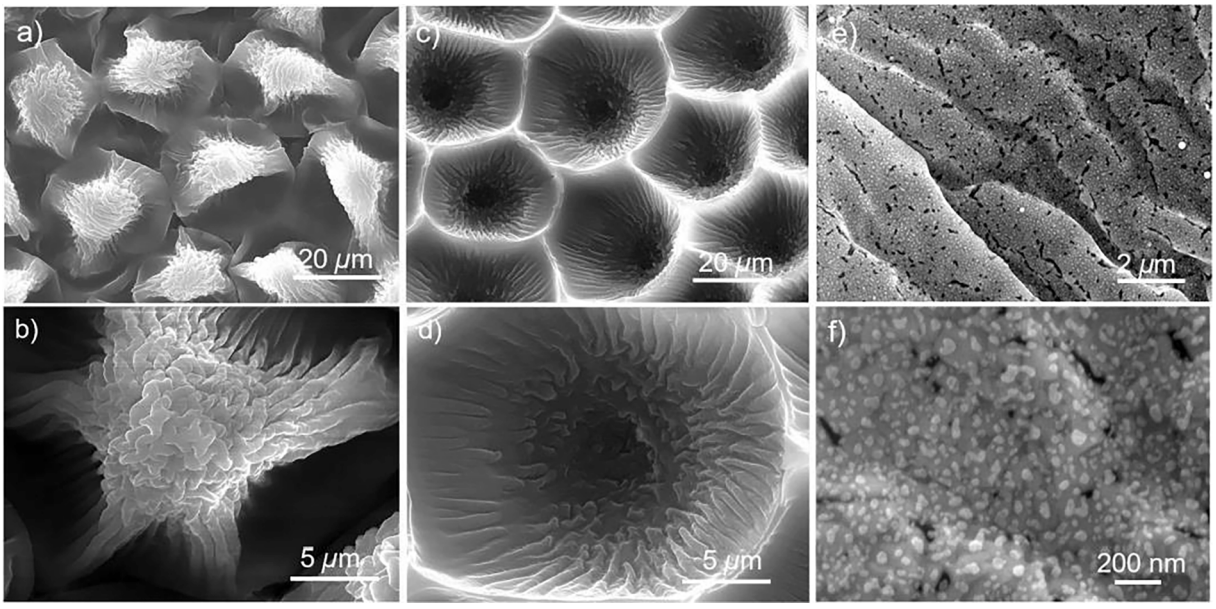

Fig. 2. SEM images of a-b) a rose petal; c-d) a PDMS replica covered with the Au/SiO_2/AuNPs structure; e)-f) AuNPs formed on the top of the biomimetic substrate after an annealing procedure.

spectra of unannealed SERS substrates based on silicone replicas of white, yellow, pink, and red rose petals are reminiscent of the spectrum from bulk gold. However, the observed absorption of spectra at wavelengths above 700 nm can be attributed to the high optical absorption capacity of percolated thin gold films [31,32]. On the other hand, the reflectance spectra of annealed SERS substrates (Fig. S5b) demonstrated the appearance of a wide resonance in the range from 550 to 630 nm, which is due to the absorption of incident light by AuNPs, surface

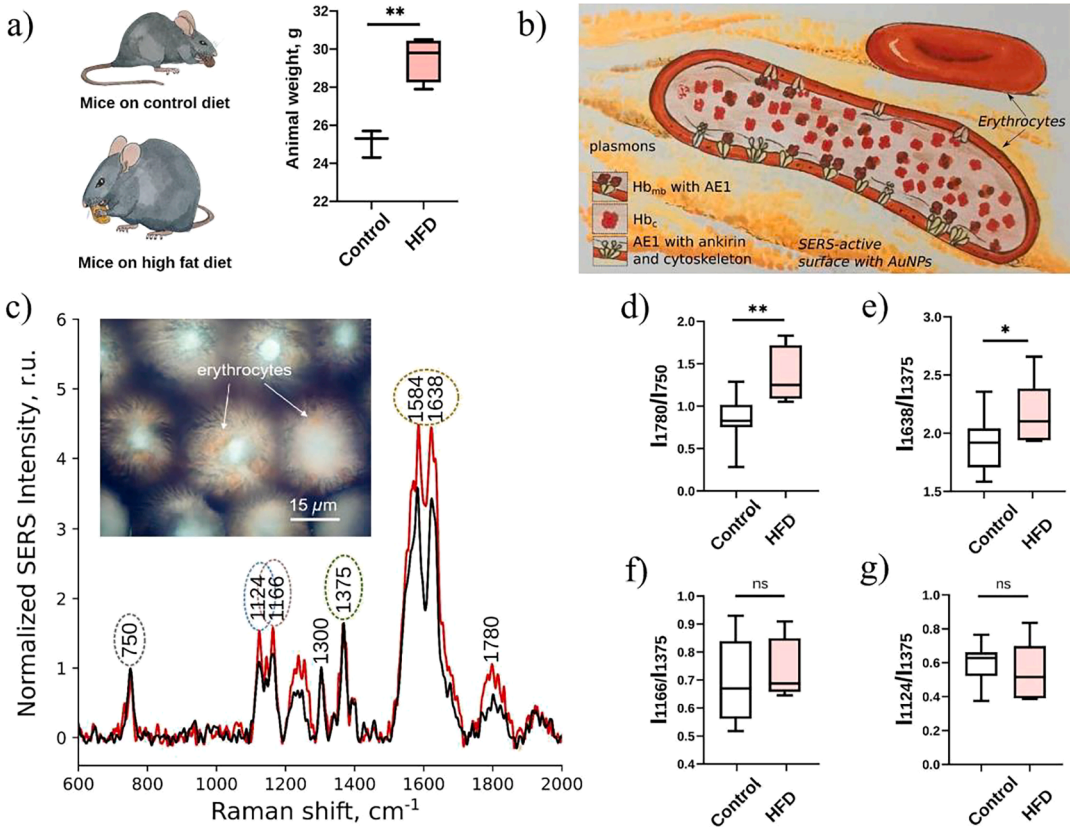

Fig. 3. The effect of HFD on body weight of mice and SERS studies of their blood properties: a) the increase in mice body weight after two-month HFD; b) schematic representation of the erythrocyte cross-section on the biomimetic SERS substrate; c) SERS spectra of 2000-times diluted blood from control mice (black spectrum) and HFD mice (red spectrum). SERS spectra are shown as mean spectra calculated from 6 independent measurements with RSDs of less than 10%; d) relative input of C═O group vibrations normalized on the total amount of Hb_m; e, f, and g) relative input of methine bridges, asymmetric pyrrole ring, and C_b-CH_3 bond vibrations normalized on symmetric pyrrole rings vibrations. *$p < 0.05$; **$p < 0.01$ (non-parametric *t*-test).

plasmon modes propagating along SiO_2-Au boundaries, and gap surface plasmon modes relatively weakly localized between AuNPs and the Au thin film. Notably, the transformation of the upper gold film into AuNPs upon annealing causes the decrease in absorption in the long wavelength region. The behavior of the obtained spectra is quite typical for such systems and well described earlier [33,34].

3.3. SERS analysis of erythrocyte membrane oxidation

Cell membranes are among first targets for ROS. Membrane oxidation may lead to the irreversible change in the cell properties and to the cell death. The lipid and protein carbonyl (C═O) group content is a commonly used marker for oxidative modification of lipids and proteins, providing significant evidence of oxidative stress in clinical samples. Generally, C═O groups in proteins are generated due to the oxidation of protein backbones and amino acid residues such as proline, arginine, lysine, and threonine by ROS molecules. C═O groups can also be a sign of lipids oxidation [35,36].

To demonstrate the applicability of the proposed SERS substrates to the detection of the oxidative stress in biological membranes, we performed experiments with erythrocytes from healthy mice subjected to the normal and high fat diets (Fig. 3a) [37]. High fat diet is known to increase the total organism weight and the amount of cholesterol affecting composition of lipids in cell plasma membranes and in lipid droplets in cell cytoplasm [37,38]. The possible negative effects of a high fat diet are widely discussed supposing the increased probability of the oxidative stress development [39,40]. Presumably, HFD could affect erythrocytes, especially their membrane and submembrane regions, due to the significant change in the blood plasma composition.

The submembrane region of erythrocytes (Fig. 3b) consists of the submembrane cytoskeleton and the membrane-bound hemoglobin (Hb_{mb}) - Hb molecules bound to the cytosolic domain of the membrane anion exchanger AE1 and located in 15–20 nm from the extracellular surface of the erythrocyte plasma membrane [27]. Besides, under various hemoglobinopathies, oxidation/degradation products of cytosolic Hb and Hb_{mb} can attach to lipids in the inner plasma membrane surface of erythrocytes.

The SERS studies of erythrocyte samples taken from mice on 2-month HFD demonstrated that SERS spectra of erythrocytes had the highest intensity and the most detailed structure on SERS substrates based on silicone replicas of red rose petals, which is due to their more highly textured surface as compared with substrates based on white, yellow, and pink rose petal replicas (Fig. S6a). The increased depth of microcavity structures and multiple submicron foldings on their walls and bottom provide better conditions for much higher Raman enhancement. Besides, optical microscope images of erythrocytes placed on microstructured SERS substrates based on red rose petal replicas demonstrated that blood cells had been effectively captured and evenly distributed on the grooved inner surface of microcavities (the insert image of Fig. 3c). As a result, SERS spectra of living erythrocytes on these substrates exhibited intensive and reproducible peaks with following maxima positions: 750, 1124, 1166, 1300, 1375, 1584, and 1638 cm^{-1} corresponding to vibrations of pyrrole rings, methine bridges, and CH_3 radicals (C_b-CH_3 bond) of heme in Hb_{mb} (Fig. 3c) [41–43]. The detailed peak assignments are given in Table S1. The observed spectrum structure is in complete agreement with our previous works [12,25–27,41]. Besides, there is a wide peak at 1780 cm^{-1} corresponding to carbonyl group C═O vibrations [35,36].

Importantly, we did not observe any SERS spectrum from erythrocytes on the smooth surface covered by spherical Au nanoparticles (Fig. S6b), demonstrating the importance of the complex morphology of the proposed SERS substrates based on rose petal replicas. Besides, the enhancement factor of these biomimetic substrates was estimated at 10^5 which is comparable with the results obtained for erythrocytes by a colloidal-based SERS technique [12].

Further, to study effect of HFD on erythrocytes, we analyzed following ratios [27]:

I_{1780}/I_{750} — the relative input of C═O group vibrations normalized on the total amount of Hb_{mb}. The ratio increase corresponds to the increase in the relative amount of C═O groups in plasma membrane proteins and lipids;

I_{1638}/I_{1375} — the relative input of methine bridges normalized on symmetric pyrrole rings vibrations. The ratio increase corresponds to the increase in the affinity of Hb to O_2;

I_{1166}/I_{1375} and I_{1124}/I_{1375} — the relative input of asymmetric pyrrole ring vibrations and C_b-CH_3 bond vibrations normalized on symmetric pyrrole ring vibrations, respectively. The ratios depend on the heme surrounding and increase with decreasing in the local protein stiffness.

We found that HFD led to the increase in I_{1780}/I_{750} ratio demonstrating the increase in the relative amount of carbonyl groups in erythrocyte membranes (Fig. 3d). We attribute this effect to the oxidation of membrane lipids as a side-effect of the HFD that is known to increase the probability of oxidative stress development [40].

We also found that the increase in the I_{1638}/I_{1375} ratio indicates a change in conformation of heme in Hb_{mb} and the increase in its affinity to O_2 (Fig. 3e). We believe that this effect can be caused by changes in the conformation of AE1 exchanger (that binds Hb_{mb}) affected by cholesterol, the amount of which increases in plasma membranes under HFD [44,45]. We did not observe changes in vibrations of C_b-CH_3 heme radicals or in the motility of heme pyrrole groups (Fig. 3f,g), which indicates the absence of significant changes in conformation of the globin-protein part of Hb_{mb}. Summarizing, we demonstrated that it is possible to monitor oxidation of plasma membrane lipids of erythrocytes and to investigate oxygen-binding properties of Hb_{sm}.

3.4. SERS-based monitoring of the lipids oxidation

To demonstrate the applicability of the proposed SERS substrates to the detection of lipids oxidation in other types of biological membranes, we performed experiments with liposomes subjected to the oxidative stress evoked by $OH^{\cdot}$ radicals from the Fenton reaction. Liposomes is a widely used experimental model of organelle and plasma membranes that can be applied to analyze the effect of various stimuli on lipids in their membrane environment. SERS spectra of liposomes prepared from the yolk lecithin consist of several intensive peaks with maxima positions at 1135 and 1520 cm^{-1} attributed to bond vibrations in beta-carotene from the yolk (Fig. 4a). The less intensive peak at 1780 cm^{-1} is attributed to C═O vibrations in membrane lipids [35].

To estimate change in the C═O group amount due to the oxidation process, we analyzed relative intensity of peak at 1780 cm^{-1} normalized on the intensity of beta-carotene peak at 1520 cm^{-1} (I_{1780}/I_{1520}) and the change in the absolute intensity of 1780 cm^{-1} peak (I_{1780}) (Fig. 4b,c). We have found that conditions of the Fenton reaction [28] caused the significant increase in the intensity of the peak at 1780 cm^{-1} and of the I_{1780}/I_{1520} ratio, which indicates the increase in the relative amount of C═O groups due to the membrane oxidation. The initiation of the oxidation stress and the lipid peroxidation in the samples under the Fenton reaction was confirmed by independent techniques [46], which demonstrated the increase in the amount of membrane degradation products (Fig. 4d) and reactive oxygen species causing lipid oxidation (Fig. S7). Thus, the relative intensity of peak at 1780 cm^{-1} corresponding to C═O group vibrations can be used for the estimation of membrane oxidation.

4. Conclusions

In this article, we presented an effective, inexpensive, and scalable biomimetic technique to produce SERS substrates for the detection of the membrane oxidation in living cells. The proposed technique is based on the use of rose petals as templates to obtain silicone substrates with microcavity structures. Such microstructures promote the capture and even distribution of blood cells on a substrate surface, which results in a

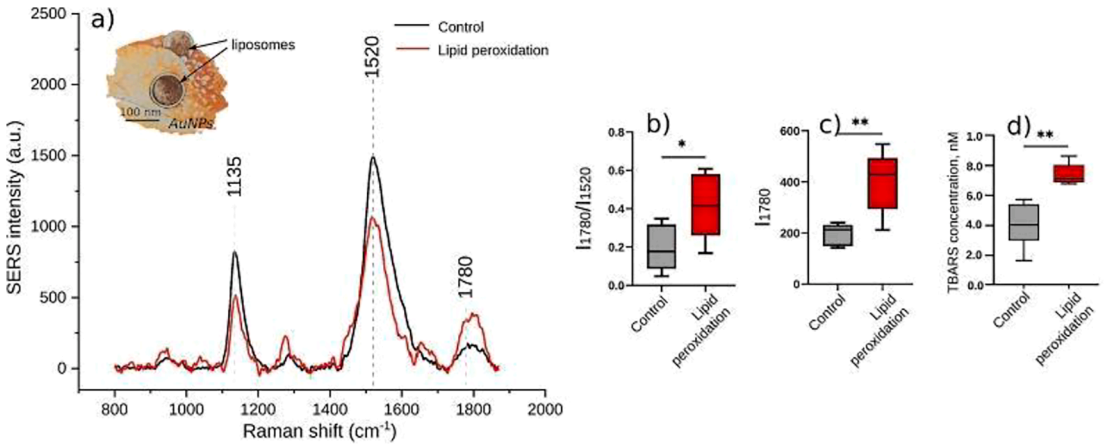

Fig. 4. Monitoring of liposome oxidation by SERS: a) SERS spectra of control liposomes (black spectrum) and liposomes after the Fenton reaction inducing lipid peroxidation (red spectrum). SERS spectra are shown as mean spectra calculated from 6 independent measurements with RSDs of less than 10%; b) and c) ratio of peak intensities I_{1780}/I_{1520} and the intensity of the peak at 1780 cm^{-1} estimated from SERS spectra of control liposomes (gray boxes) and liposomes under oxidation evoked by the Fenton reaction (red boxes); d) concentration of lipid peroxidation products in the control (gray box) and in the oxidized (red box) liposome samples. *p < 0.05; **p < 0.01 (non-parametric *t*-test).

SERS signal of high reproducibility all over a substrate surface. Besides, the microcavities covered with AuNPs provide a close contact of plasmonic nanoparticles with living erythrocytes. As a result, the high intensive SERS spectra of membrane-bound hemoglobin in its natural cellular environment can be obtained to estimate its conformation and oxygen-binding properties. In addition, the proposed SERS-active substrates provide intensive and stable enhancement of Raman scattering from C═O groups in lipids and proteins of biomembranes, which can be used to evaluate membrane oxidation and the oxidative stress development. Overall, the proposed biomimetic SERS substrates demonstrate high efficiency for a single-cell analysis and detection of even early signs of the oxidative stress in cell membranes, which is highly promising for the early diagnostics of various metabolic diseases such as diabetes, hypertension, obesity, etc.

CRediT authorship contribution statement

M. Barshutina: Conceptualization, Methodology, Investigation, Validation, Data curation, Writing – original draft, Writing – review & editing. **N. Doroshina:** Investigation. **A. Baizhumanov:** Investigation. **E. Nikelshparg:** Investigation. **A. Fedotova:** Resources. **A. Popov:** Resources. **A. Semyanov:** Resources. **D. Yakubovsky:** Investigation. **G. Tselikov:** Investigation. **O. Luneva:** Investigation. **I. Kirilyuk:** Investigation. **G. Maksimov:** Funding acquisition, Project administration. **V. Volkov:** Funding acquisition, Project administration, Supervision. **A. Arsenin:** Project administration, Supervision, Resources. **N. Brazhe:** Conceptualization, Investigation, Methodology, Formal analysis, Visualization, Data curation, Writing – review & editing. **S. Novikov:** Conceptualization, Methodology, Investigation, Formal analysis, Visualization, Data curation, Writing – review & editing.

Declaration of Competing Interest

The authors declare that they have no known competing financial interests or personal relationships that could have appeared to influence the work reported in this paper.

Data availability

Data will be made available on request.

Acknowledgment

This work was supported by the Ministry of Science and Higher Education of the Russian Federation (Agreement No. 075-15-2021-606). AB, AF and NB acknowledge support from the Russian Scientific Foundation (22-14-00033) for SERS experiments with erythrocytes and liposomes.

Appendix A. Supplementary data

Supplementary data to this article can be found online at https://doi.org/10.1016/j.apsusc.2023.157281.

References

[1] M. Katerji, M. Filippova, P. Duerksen-Hughes, Approaches and methods to measure oxidative stress in clinical samples: research application in the cancer field, Oxid. Med. Cell. Longev. 2019 (2019) 1279250, https://doi.org/10.1155/2019/1279250.

[2] J. Herman, Y. Zhang, V. Castranova, S.L. Neal, Emerging technologies for optical spectral detection of reactive oxygen species, Anal. Bioanal. Chem. 410 (24) (2018) 6079–6095, https://doi.org/10.1007/s00216-018-1233-1.

[3] M.P. Murphy, H. Bayir, V. Belousov, C.J. Chang, K.J.A. Davies, M.J. Davies, T. P. Dick, T. Finkel, H.J. Forman, Y. Janssen-Heininger, D. Gems, V.E. Kagan, B. Kalyanaraman, N.G. Larsson, G.L. Milne, T. Nystrom, H.E. Poulsen, R. Radi, H. Van Remmen, P.T. Schumacker, P.J. Thornalley, S. Toyokuni, C.C. Winterbourn, H. Yin, B. Halliwell, Guidelines for measuring reactive oxygen species and oxidative damage in cells and in vivo, Nat. Metab. 4 (6) (2022) 651–662, https://doi.org/10.1038/s42255-022-00591-z.

[4] W.R. Premasiri, Y. Chen, J. Fore, A. Brodeur, L.D. Ziegler, Chapter 10 - SERS biomedical applications: diagnostics, forensics, and metabolomic, in: J. Laane (Ed.), Frontiers and advances in molecular spectroscopy, Elsevier, 2018, pp. 327–367.

[5] R. Pilot, R. Signorini, C. Durante, L. Orian, M. Bhamidipati, L.A. Fabris, Review on surface-enhanced Raman scattering, Biosensors 9 (2) (2019) 57, https://doi.org/10.3390/bios9020057.

[6] J. Langer, D. Jimenez de Aberasturi, J. Aizpurua, R.A. Alvarez Puebla, B. Auguie, J. J. Baumberg, G.C. Bazan, S.E.J. Bell, A. Boisen, A.G. Brolo, et al., Present and future of surface-enhanced Raman scattering, ACS Nano 14 (1) (2020) 28–117, https://doi.org/10.1021/acsnano.9b04224.

[7] J.M. Romo-Herrera, K. Juarez-Moreno, L. Guerrini, Y. Kang, N. Feliu, W.J. Parak, R.A. Alvarez-Puebla, Paper-based plasmonic substrates as surface-enhanced Raman scattering spectroscopy platforms for cell culture applications, Materials Today Bio 11 (2021), 100125, https://doi.org/10.1016/j.mtbio.2021.100125.

[8] G. Kuku, M. Altunbek, M. Culha, Surface-enhanced Raman scattering for label-free living single cell analysis, Anal. Chem. 89 (21) (2017) 11160–11166, https://doi.org/10.1021/acs.analchem.7b03211.

[9] Y. Shen, J. Yue, W. Xu, S. Xu, Recent progress of surface-enhanced Raman spectroscopy for subcellular compartment analysis, Theranostics 11 (10) (2021) 4872–4893, https://doi.org/10.7150/thno.56409.

[10] J. Ando, K. Fujita, N.I. Smith, S. Kawata, Dynamic SERS imaging of cellular transport pathways with endocytosed gold nanoparticles, Nano Lett. 11 (12) (2011) 5344–5348, https://doi.org/10.1021/nl202877r.
[11] Y. Zhang, D. Jimenez de Aberasturi, M. Henriksen-Lacey, J. Langer, L.M. Liz-Marzán, Live-cell surface-enhanced Raman spectroscopy imaging of intracellular pH: from two dimensions to three dimensions, ACS Sensors 5 (10) (2020) 3194–3206, https://doi.org/10.1021/acssensors.0c01487.
[12] N.A. Brazhe, E.Y. Parshina, V.V. Khabatova, A.A. Semenova, A.R. Brazhe, A. I. Yusipovich, A.S. Sarycheva, A.A. Churin, E.A. Goodilin, G.V. Maksimova, O. V. Sosnovtseva, Turning SERS for living erythrocytes: focus on nanoparticle size and plasmon resonance position, J. Raman Spectrosc. 44 (5) (2013) 686–694, https://doi.org/10.1002/jrs.4274.
[13] B. Ren, A.I. Pérez-Jiménez, D. Lyu, Z. Lu, G. Liu, Surface-enhanced Raman spectroscopy: benefits, trade-offs and future developments, Chem. Sci. 11 (2020) 4563, https://doi.org/10.1039/d0sc00809e.
[14] N.A. Brazhe, A.B. Evlyukhin, E.A. Goodilin, A.A. Semenova, S.M. Novikov, S. I. Bozhevolnyi, B.N. Chichkov, A.S. Sarycheva, A.A. Baizhumanov, E. I. Nikelshparg, L.I. Deev, E.G. Maksimov, G.V. Maksimov, O.V. Sosnovtseva, Probing cytochrome c in living mitochondria with surface-enhanced Raman spectroscopy, Sci. Rep. 5 (2015) 13793, https://doi.org/10.1038/srep13793.
[15] Q. Jin, M. Li, B. Polat, S.K. Paidi, A. Dai, A. Zhang, J.V. Pagaduan, I. Barman, D. H. Gracias, Mechanical trap surface-enhanced Raman spectroscopy for three-dimensional surface molecular imaging of single live cells, Angew. Chem. Int. Ed. 56 (14) (2017) 3822–3826, https://doi.org/10.1002/anie.201700695.
[16] I. Rigo, M. Veres, T. Vaczi, E. Holczer, O. Hakkel, A. Deak, P. Furjes, Preparation and characterization of perforated SERS active array for particle trapping and sensitive molecular analysis, Biosensors 9 (3) (2019) 93, https://doi.org/10.3390/bios9030093.
[17] C.C. Ho, K. Zhao, T. Lee, Quasi-3D gold nanoring cavity arrays with high-density hot-spots for SERS applications via nanosphere lithography, Nanoscale 6 (15) (2014) 8606–8611, https://doi.org/10.1039/c4nr00902a.
[18] R. Sakalys, K.W. Kho, T.E. Keyes, A reproducible, low cost microfluidic microcavity array SERS platform prepared by soft lithography from a 2 photon 3D printed template, Sens. Actuators B 340 (2021), 129970, https://doi.org/10.1016/j.snb.2021.129970.
[19] S.-C. Luo, K. Sivashanmugan, J.-D. Liao, C.-K. Yao, H.-C. Peng, Nanofabricated SERS-active substrates for single-molecule to virus detection in vitro: A review, Biosens. Bioelectron. 61 (2014) 232–240, https://doi.org/10.1016/j.bios.2014.05.013.
[20] L. Yao, P. Dai, L. Ouyang, L. Zhu, A sensitive and reproducible SERS sensor based on natural lotus leaf for paraquat detection, Microchem. J. 160B (2021), 105728, https://doi.org/10.1016/j.microc.2020.105728.
[21] S.-Y. Chou, C.-C. Yu, Y.-T. Yen, K.-T. Lin, H.-L. Chen, W.-F. Su, Romantic story or Raman scattering? Rose petals as ecofriendly, low-cost substrates for ultrasensitive surface-enhanced Raman scattering, Anal. Chem. 87 (12) (2015) 6017–6024, https://doi.org/10.1021/acs.analchem.5b00551.
[22] U.T. Pham, Q.H.T. Phan, L.P. Nguyen, P.D. Luu, T.D. Doan, H.T. Trinh, C.T. Dinh, T.V. Nguyen, T.Q. Tran, D.X. Le, T.N. Pham, T.D. Le, D.T. Nguyen, Rapid quantitative determination of multiple pesticide residues in mango fruits by surface-enhanced Raman spectroscopy, Processes 10 (3) (2022) 442, https://doi.org/10.3390/pr10030442.
[23] P. Kumar, R. Khosla, M. Soni, D. Deva, S.K. Sharma, A highly sensitive, flexible SERS sensor for malachite green detection based on Ag decorated microstructured PDMS substrate fabricated from Taro leaf as template, Sens. Actuators B 246 (2017) 477–486, https://doi.org/10.1016/j.snb.2017.01.202.
[24] V. Sharma, V. Krishnan, Fabrication of highly sensitive biomimetic SERS substrates for detection of herbicides in trace concentrations, Sens. Actuators B 262 (2018) 710–719, https://doi.org/10.1016/j.snb.2018.01.230.
[25] A.A. Semenova, N.A. Brazhe, E.Y. Parshina, V.K. Ivanov, G.V. Maksimov, E. A. Goodilin, Aqueous diaminsilver hydroxide as a precursor of pure silver nanoparticles for SERS probing of living erythrocytes, Plasmonic 9 (2014) 227–235, https://doi.org/10.1007/s11468-013-9616-9.
[26] A.A. Semenova, N.A. Brazhe, E.Y. Parshina, A.S. Sarycheva, G.V. Maksimov, E. A. Goodilin, A new route for SERS analysis of intact erythrocytes using polydisperse silver nanoplatelets on biocompatible scaffolds, RSC Adv. 6 (88) (2016) 85156–85164, https://doi.org/10.1039/C6RA20372H.
[27] E.I. Nikelshparg, A.A. Baizhumanov, Z.V. Bochkova, S.M. Novikov, D. I. Yakubovsky, A.V. Arsenin, V.S. Volkov, E.A. Goodilin, A.A. Semenova, O. Sosnovtseva, G.V. Maksimov, N.A. Brazhe, Detection of hypertension-induced changes in erythrocytes by SERS nanosensors, Biosensors 12 (2022) 32, https://doi.org/10.3390/bios12010032.
[28] A.N. Semenov, D.A. Gvozdev, D.V. Zlenko, E.A. Protasova, A.R. Khashimova, E. Y. Parshina, A.A. Baizhumanov, N.Y. Lotosh, E.E. Kim, Y.N. Kononevich, A. A. Pakhomov, A.A. Selishcheva, N.N. Sluchanko, E.A. Shirshin, E.G. Maksimov, Modulation of membrane microviscosity by protein-mediated carotenoid delivery as revealed by time-resolved fluorescence anisotropy, Membranes 12 (2022) 905, https://doi.org/10.3390/membranes12100905.
[29] E. Nagababu, J.M. Rifkind, S. Boindala, L. Nakka, Assessment of antioxidant activity of Eugenol in vitro and in vivo, Free Radicals Antioxidant Protocols 610 (2010) 165–180, https://doi.org/10.1007/978-1-60327-029-8_10.
[30] S.I. Dikalov, Y.F. Polienko, I. Kirilyuk, Electron paramagnetic resonance measurements of reactive oxygen species by cyclic hydroxylamine spin probes, Antioxidants Redox Signaling 28 (15) (2018) 1433–1443, https://doi.org/10.1089/ars.2017.7396.
[31] M.K. Tatmyshevskiy, D.I. Yakubovsky, O.O. Kapitanova, V.R. Solovey, A. A. Vyshnevyy, G.A. Ermolaev, Y.A. Klishin, M.S. Mironov, A.A. Voronov, A. V. Arsenin, V.S. Volkov, S.M. Novikov, Hybrid metal-dielectric-metal sandwiches for SERS applications, Nanomaterials 11 (12) (2021) 3205, https://doi.org/10.3390/nano11123205.
[32] Y. Lu, W. Dong, Z. Chen, A. Pors, Z. Wang, S.I. Bozhevolnyi, Gap-plasmon based broadband absorbers for enhanced hot-electron and photocurrent generation, Sci. Rep. 6 (2016) 30650, https://doi.org/10.1038/srep30650.
[33] A.S. Roberts, S.M. Novikov, Y. Yang, Y. Chen, S. Boroviks, J. Beermann, N. A. Mortensen, S.I. Bozhevolnyi, Laser writing of bright colors on near-percolation plasmonic reflector arrays, ACS Nano 13 (1) (2019) 71–77, https://doi.org/10.1021/acsnano.8b07541.
[34] S.M. Novikov, S. Boroviks, A.B. Evlyukhin, D.E. Tatarkin, A.V. Arsenin, V. S. Volkov, S.I. Bozhevolnyi, Fractal shaped periodic metal nanostructures atop dielectric-metal substrates for SERS applications, ACS Photonics 7 (7) (2020) 1708–1715, https://doi.org/10.1021/acsphotonics.0c00257.
[35] S. Luqman, S.I. Rizvi, Protection of lipid peroxidation and carbonyl formation in proteins by capsaicin in human erythrocytes subjected to oxidative stress, Phytotherapy Res. 20 (4) (2006) 303–306, https://doi.org/10.1002/ptr.1861.
[36] A. Lambert, F. Bougrioua, O. Abbas, M. Courty, M. El Marssi, V. Faivre, S. Bresson, Temperature dependent Raman and X-ray diffraction studies of anhydrous milk fat, Food Chem. 267 (2018) 187–195, https://doi.org/10.1016/j.foodchem.2017.09.006.
[37] A. Popov, N. Brazhe, A. Fedotova, A. Tiaglik, M. Bychkov, K. Morozova, A. Brazhe, D. Aronov, E. Lyukmanova, N. Lazareva, L. Li, E. Ponimaskin, A. Verkhratsky, A. Semyanov, A high-fat diet changes astrocytic metabolism to promote synaptic plasticity and behavior, Acta Physiol. 236 (1) (2022) e13847.
[38] S. Nishikawa, A. Yasoshima, K. Doi, H. Nakayama, K. Uetsuka, Involvement of sex, strain and age factors in high fat diet-induced obesity in C57BL/6J and BALB/cA mice, Exp. Anim. 56 (4) (2007) 263–272, https://doi.org/10.1538/expanim.56.263.
[39] H. Yimin, S. Furumaki, T. Matsuoka, M. Sakurai, S. Kohanawa, Y. Zhao, N. Kuge, H. Tamaki, Chiba, A novel murine model for non-alcoholic steatohepatitis developed by combination of a high-fat diet and oxidized low-density lipoprotein, Lab. Invest. 92 (2) (2012) 265–281, https://doi.org/10.1038/labinvest.2011.159.
[40] B.L. Tan, M.E. Norhaizan, Effect of high-fat diets on oxidative stress, cellular inflammatory response and cognitive function, Nutrients 11 (11) (2019) 2579, https://doi.org/10.3390/nu11112579.
[41] N.A. Brazhe, S. Abdali, A.R. Brazhe, O.G. Luneva, N.Y. Bryzgalova, E.Y. Parshina, O.V. Sosnovtseva, G.V. Maksimov, New insight into erythrocyte through in vivo surface-enhanced Raman spectroscopy, Biophys. J. 97 (12) (2009) 3206–3214, https://doi.org/10.1016/j.bpj.2009.09.029.
[42] T.G. Spiro, T.C. Strecas, Resonance Raman spectra of hemoglobin and cytochrome c: inverse polarization and vibronic scattering, Proc. Natl. Acad. Sci. 69 (9) (1972) 2622–2626, https://doi.org/10.1073/pnas.69.9.2622.
[43] S.Z. Hu, K.M. Smith, T.G. Spiro, Assignment of protoheme resonance Raman spectrum by heme labeling in myoglobin, J. Am. Chem. Soc. 118 (50) (1996) 12638–12646, https://doi.org/10.1021/ja962239e.
[44] K.R. Shanmugasundaram, A. Visvanathan, K. Dhandapani, N. Srinivasan, P. Rasappan, R. Gilbert, S. Alladi, S. Kancharla, N. Vasanthi, Effect of high-fat diet on cholesterol distribution in plasma lipoproteins, cholesterol esterifying activity in leukocytes, and erythrocyte membrane components studied: importance of body weight, Am. J. Clin. Nutr. 44 (6) (1986) 805–815, https://doi.org/10.1093/ajcn/44.6.805.
[45] D.D. Vecchis, R.A.F. Reithmeier, A.C. Kalli, Molecular simulations of intact anion exchanger 1 reveal specific domain and lipid interactions, Biophys. J. 117 (7) (2019) 1364–1379, https://doi.org/10.1016/j.bpj.2019.08.029.
[46] A.V. Graf, A.A. Baizhumanov, M.V. Maslova, Y.V. Krushinskaya, A.S. Maklakova, N.A. Sokolova, A.A. Kamensky, Effect of acute hypoxia on oxidative stress indices in rat offspring at different stages of gestation, Mosc. Univ. Biol. Sci. Bull. 77 (2) (2022) 104–111, https://doi.org/10.3103/S0096392522020043.